ELSEVIER

Neurobiology of Aging 34 (2013) 694–705

NEUROBIOLOGY OF AGING

www.elsevier.com/locate/neuaging

Evolution of source EEG synchronization in early Alzheimer's disease

Maria G. Knyazeva[a,b,*], Cristian Carmeli[a], Alireza Khadivi[c], Joseph Ghika[a], Reto Meuli[b,d], Richard S. Frackowiak[a]

[a] LREN, Department of Clinical Neuroscience, Centre Hospitalier Universitaire Vaudois (CHUV), and University of Lausanne, Lausanne, Switzerland
[b] Department of Radiology, Centre Hospitalier Universitaire Vaudois (CHUV), and University of Lausanne, Lausanne, Switzerland
[c] LANOS, EPFL Lausanne, Switzerland
[d] CIBM, CHUV Unit, Lausanne, Switzerland

Received 21 February 2012; received in revised form 29 June 2012; accepted 11 July 2012

Abstract

Alzheimer's disease (AD) disrupts functional connectivity in distributed cortical networks. We analyzed changes in the S-estimator, a measure of multivariate intraregional synchronization, in electroencephalogram (EEG) source space in 15 mild AD patients versus 15 age-matched controls to evaluate its potential as a marker of AD progression. All participants underwent 2 clinical evaluations and 2 EEG recording sessions on diagnosis and after a year. The main effect of AD was hyposynchronization in the medial temporal and frontal regions and relative hypersynchronization in posterior cingulate, precuneus, cuneus, and parietotemporal cortices. However, the S-estimator did not change over time in either group. This result motivated an analysis of rapidly progressing AD versus slow-progressing patients. Rapidly progressing AD patients showed a significant reduction in synchronization with time, manifest in left frontotemporal cortex. Thus, the evolution of source EEG synchronization over time is correlated with the rate of disease progression and should be considered as a cost-effective AD biomarker.

Keywords: Alzheimer's disease; Functional connectivity; Hypersynchronization; Hyposynchronization; Prognosis; S-estimator; EEG; Clinical biomarker

1. Introduction

What happens to neuronal synchronization in Alzheimer's disease (AD)? The question is of primary importance because synchronization between spatially remote neurophysiological events is thought to be a principal mechanism of effective and functional connectivity (EC and FC) that is of direct and indirect interactions between spatially distributed brain areas (Friston et al., 1993; Singer, 1999). Electroencephalogram (EEG) reports describing moderate to severe AD suggest a progressive degradation similar to that in structural connectivity (Babiloni et al., 2006a; Koenig et al., 2005; Kramer et al., 2007; Lizio et al., 2011; Stam et al., 2005). However, findings in preclinical and early AD show a more complicated picture that includes both strengthening and weakening of FC estimated with functional magnetic resonance imaging (fMRI) (Damoiseaux et al., 2012; Sperling et al., 2010; Wang et al., 2007; Zhang et al., 2010) or EEG synchronization (Knyazeva et al., 2010; Rossini et al., 2006) at rest and with activation. New evidence based on a mouse model of AD suggests these phenomena correlate with the accumulation of β-amyloid, which is associated with dysfunction of inhibitory interneurons that, in turn, could augment synchronicity between pyramidal cells (Palop and Mucke, 2010). There are findings in human AD compatible with such a hypothesis.

A disproportionate weakening of EC, ascribed to lost inhibitory modulatory connections, has been demonstrated in mild AD (Rytsar et al., 2011). In this study, EC in AD patients and matched controls was analyzed by means of dynamic causal modeling of fMRI time series in a visual integration task. The inhibitory effects exerted by extrastri-

* Corresponding author at: LREN, NLG, BH07, CHUV, 1011 Lausanne, Switzerland. Tel.: +41 21 314 32 31; fax: +41 21 314 12 90.
E-mail address: Maria.Knyazeva@chuv.ch (M. Knyazeva).

0197-4580/$ – see front matter © 2013 Elsevier Inc. All rights reserved.
http://dx.doi.org/10.1016/j.neurobiolaging.2012.07.012

ate on primary visual areas associated with interhemispheric integration of a visual stimulus were significantly weakened in AD patients. The same AD patients were also characterized by an abnormal landscape of intraregional EEG synchronization that was impaired in frontotemporal regions of the left hemisphere and augmented in the posterior temporal, parietal, and occipital cortices of both hemispheres (Knyazeva et al., 2010). These features discriminated patients from controls with an accuracy of up to 94%. Anterior hyposynchronization and posterior hypersynchronization correlated with individual Mini Mental State Examination (MMSE) scores, thus linking both types of FC change to AD-associated cognitive decline.

Posterior hypersynchronization was much more pronounced in early-onset AD patients and in those with short disease duration (Knyazeva et al., 2010). The literature suggests further changes in moderate to severe AD manifesting predominantly as hyposynchronization compared with matched controls (Koenig et al., 2005; Lizio et al., 2011). Therefore, the evolution of AD-associated neurodegeneration causes qualitative changes in EEG synchronization, and hypersynchronization is a hallmark of early or even preclinical AD. However, this sequence of events is presently based on extrapolation from cross-sectional studies. Proof from formal longitudinal studies is required. Here we present a longitudinal study over a year starting from the clinical diagnosis of AD. To assay the dynamics of synchronization within this period, we apply whole-brain mapping of multivariate intraregional FC in EEG source space using the S-estimator, a multivariate measure exploiting dimensionality shrinking—a theoretical consequence of synchronization phenomena (see Section 2.4.)—for the assessment of synchronization within a set of multivariate measurements (Carmeli et al., 2005).

2. Methods

2.1. Patients and control subjects

Fifteen newly diagnosed AD patients (3 women and 12 men; Table 1a) were recruited from the Memory Clinic of the Neurology Service (CHUV, Lausanne). Fifteen control subjects (9 women and 6 men) were volunteers enrolled among partners, caregivers, or family members. The patient and control groups differed neither in age nor in level of education. At baseline, this population overlapped with the population reported in our cross-sectional study (Knyazeva et al., 2010), where we analyzed surface EEG in newly diagnosed AD patients. Eleven patients and 11 controls were common across these 2 studies. All participants gave written informed consent. All procedures conformed to the Declaration of Helsinki (1964) of the World Medical Association concerning human experimentation and were approved by the local Ethics Committee of Lausanne University.

Table 1
Demographic and clinical characteristics of the AD and control subjects and of the relatively stable and fast-progressing AD patients

a. Demographic and clinical characteristics of the AD and control groups

Group	AD patients	Control subjects	*p*
Subjects, *n*	15	15	—
Gender, M/F	12/3	6/9	—
Age (y)	68.7 ± 5.1	67.6 ± 5.0	NS
CO (y)	1.9 ± 0.2	1.6 ± 0.2	NS
EEG observation interval (*months*)	12.4 ± 0.7	12.2 ± 0.6	NS
MMSE at baseline	22.6 ± 1.1	28.5 ± 1.2	0.001
MMSE in the end of CO	18.1 ± 2.1	28.5 ± 1.2	0.001
Disease duration (y)	3.8 ± 0.5	—	—
Education[a]	2.2 ± 0.2	2.4 ± 0.1	NS

b. Demographic and clinical characteristics of the relatively stable and progressing AD subgroups

	Fast-progressing AD patients	Slow-progressing AD patients	
Number of subjects	8	7	—
Gender M/F	5/3	7/0	—
Age (y)	71.9 ± 4.0	65.6 ± 3.1	NS
CO (y)	1.8 ± 0.3	2.1 ± 0.3	NS
EEG observation interval (*months*)	12.1 ± 0.9	12.6 ± 1.0	NS
MMSE at baseline	20.5 ± 1.5	24.6 ± 1.4	NS
MMSE in the end of CO	11.9 ± 2.1	24.3 ± 1.8	0.001
Disease duration	4.1 ± 0.7	3.6 ± 0.8	NS
Education[a]	2.3 ± 0.3	2.1 ± 0.3	NS

Second and third columns present group characteristics (mean ± standard error). Fourth column presents *p*-values for the statistical significance of the between-group differences. The duration of the disease was determined as the time in years between the onset of recent episodic memory symptoms reported by the patient or relatives and the date of neuropsychological examination, as recommended in the American Academy of Neurology Practice Handbook (Practice parameter for diagnosis and evaluation of dementia (summary statement)).

Key: AD, Alzheimer's disease; CO, clinical observation; EEG, electroencephalogram; F, female; M, male; MMSE, Mini Mental State Examination; NS, not significant.

[a] Educational status was determined by 3 categories: 1, primary/secondary school without, or with short (< 3 years) professional training; 2, primary/secondary school with professional training (> 3 years); and 3, high school and tertiary education.

The clinical diagnosis of probable AD was made according to the National Institute of Neurological and Communicative Disorders and Stroke and the Alzheimer's Disease and Related Disorders Association criteria (McKhann et al., 1984), allowing a certainty in the diagnosis of about 80%–85%. Cognitive functions were assessed with the MMSE (Folstein et al., 1975) and with a detailed standardized neuropsychological assessment scale validated for a francophone population (Puel and Hugonot-Diener, 1996). The impact of cognitive impairment on daily life was evaluated with the Basic Activity of Daily Living Scale (Katz, 1983), and with the Instrumental Activity of Daily Living Scale (Lawton and Brody, 1969). To improve compatibility across studies the stage of dementia was determined both by the Functional Assessment Staging (Scaln and Reisberg, 1992)

and Clinical Dementia Rating (Morris, 1993) scales. For this study we selected patients with mild dementia at baseline (Functional Assessment Staging score, 3–4; and Clinical Dementia Rating score, 0.5–1).

Clinical laboratory investigations and diagnostic neuroimaging (computed tomography or magnetic resonance imaging [MRI] and metrizamide single-photon emission computed tomography) were performed to exclude other causes of dementia. Exclusion criteria were severe physical illness, psychiatric or other neurological disorders associated with potential cognitive dysfunction, other dementing conditions (frontotemporal dementia, dementia associated with Parkinsonism, Lewy body disease, pure vascular or prion-associated dementia, etc.), alcohol/drug abuse, and regular use of neuroleptics, antidepressants with anticholinergic action, benzodiazepines, stimulants, or β-blockers. To confirm the absence of psychoactive drug use, or other diseases that interfere with cognitive functions, potential control subjects underwent a brief clinical interview, including the MMSE, and a brain MRI scan. Only individuals with no cognitive complaints and a score ≥ 28 for a high and ≥ 26 for a low level of education were accepted as controls.

All the subjects are participants of a 3-year longitudinal study (Swiss National Foundation, Grant number 320030-127538/1), which includes clinical, EEG, and MRI evaluations on an annual basis. Here we report the EEG results at 1 year from AD diagnosis. The mean time between EEG sessions was 12.4 ± 0.7 (mean $\pm$ standard error) months for patients and 12.2 ± 0.6 months for controls. All patients were treated with a cholinesterase inhibitor in this period, all but 1 slow and 1 rapidly regressing patient received an antidepressant and none of the control subjects was medicated. Considering that (1) the effects of cholinesterase inhibitors on AD progression are very limited (Birks, 2006), (2) antidepressants have never affected AD progression or MMSE scores, and (3) that medication is given to reduce the differences between controls and patients, medication-related false positives are very unlikely.

2.2. EEG recording and preprocessing

The EEG data were collected with subjects sitting relaxed with eyes closed. The EEGs were recorded with a 128-channel Geodesic Sensor Net (Electrical Geodesic, Inc., Eugene, OR, USA) for 3–4 minutes. All electrode impedances were kept under 30 kΩ—much lower than recommended (50 kΩ) for the high-input impedance amplifiers. The recordings were made with vertex references using a low-pass filter set to 100 Hz. The signals were digitized at a rate of 500 samples per second with a 12-bit analogue-to-digital converter. They were filtered (band-pass of 1–50 Hz) and rereferenced against the common average. The latter operation has the benefit of providing reference-independent inverse solutions (Pascual-Marqui, 2009).

To achieve greater confidence in the synchronization estimates, the signals were segmented into nonoverlapping 1-second epochs. Using short segments for analysis allowed us to record 155 ± 17 (mean $\pm$ standard error) artifact-free epochs for patients and 142 ± 18 for controls. Artifacts in all channels were edited off-line: first automatically, based on an absolute voltage threshold (100 μV) and on a transition threshold (50 μV), and then on the basis of a thorough visual inspection. The sensors producing artifacts more than 20% of the recording time were corrected using a bad channel replacement tool (Net Station 4.2, Electrical Geodesic, Inc.).

2.3. LAURA—bioelectromagnetic inverse imaging

Local auto-regressive average (LAURA) is a method used to image generators of scalp-recorded electromagnetic activity (Grave de Peralta Menendez et al., 2001). It provides a distributed linear inverse solution based on a local auto-regressive average model of unknown current density in the brain. Its interpolation coefficients depend upon a power of the Euclidean distance between current density locations of interest and their neighbors. We computed the LAURA-based EEG solution for a head model with 4024 solution points isotropically distributed at 6 mm intervals within the gray matter compartment of the Montreal Neurological Institute's (MNI) average brain (Mazziotta et al., 1995). These solution points span superficial and deep gray matter, except the cerebellum. The head model was coregistered with EEG electrode coordinates from MNI space, and the lead-field matrix was computed via the 3 shell SYmmetric Spherical Head Model with Anatomical Constrains (Grave de Peralta Menendez et al., 2006). This method has been successfully used in clinical and experimental studies and results in localization precision that is comparable with realistic boundary element models (Guggisberg et al., 2011). At each solution point, 3-D current density time series were produced. To avoid excessive computational demands and uncertainties in the interpretation of synchronization maps along the 3 components of current density vectors, for subsequent data analysis we considered the modulus or intensity of the vectors, thus discarding their directionality.

2.4. Measuring multivariate source EEG synchronization

Synchronization occurs when there is a correlation of activity between a number of systems due to either a coupling configuration or driven by an external source (Brown and Koçarev, 2000). In order to estimate the amount of synchrony defined by distances (volumes) of interest (see below), that is between multiple neighboring sources, we exploited the S-estimator (for a discussion of this multivariate approach and numerical validation of the method, see Carmeli, 2006; Carmeli et al., 2005). The S-estimator exploits the theoretical consequences of synchronization phenomena to quantify the synchronization of a set of signals. The observable dimensionality of a network of dynamic systems decreases as a result of interactions among its

elements (Brown and Koçarev, 2000). The S-estimator indirectly measures this synchronization-induced contraction of observed dimensionality by measuring the eigenvalue dispersion (entropy) in the 0-lag correlation matrix of a multivariate set of signals. The S-estimator can be applied to multivariate time series or to phase-space embedded multivariate data. The latter involves the estimation of 2 parameters for each solution point, namely time lag and embedding dimension (Carmeli et al., 2005). Because such estimations are time-consuming in a large-scale setting, we opted for the most simple approach, that of considering the nonphase-space embedded time series.

Given a K-variate time series, the S-estimator is defined as:

$$S = 1 - \frac{E(\lambda)}{\log(K)}$$

where λ designates the normalized eigenvalues of the 0-lag correlation matrix of the K-variate time series, and E(λ) is their Shannon entropy. When all normalized eigenvalues are roughly of the same value (maximum dispersion of eigenvalues), all the state-space dimensions are almost equally visited; in this case E(λ) is maximum [close to log(K)], consequently S is close to 0, meaning no contraction of the observed dimensionality, i.e., no synchronization. Alternatively, when nearly all normalized eigenvalues are roughly 0 and only a few are not (minimal dispersion), only a few state-space dimensions are visited; in this case E(λ) is minimal (close to 0), consequently S is close to 1, meaning maximal contraction of the observed dimensionality and complete synchronization. Thus, the S-estimator is a multivariate measure that fits the structure of source EEG by allowing a reconstruction of the whole-brain topography of synchronization.

2.5. Whole-brain topography

Whole-brain maps were obtained by applying the S-estimator to 4024 volumes of interest. Each volume of interest corresponded to a sphere of 3 cm in radius centered on a solution point. On average, a volume of interest included about K = 200 sources, and embraced the range of distances spanned by short corticocortical association fibers (Schuz and Braitenberg, 2002), which are demyelinated in early AD patients (Fornari et al., 2012). To reduce the computational burden and to avoid the issue of multiple comparisons when assessing synchronization maps for several EEG frequency bands, we applied the S-estimator to broadband source EEG signals. This approach seemed to be optimal for achieving the aims of our study given the further fact that in previous work similar synchronization landscapes were found across conventional EEG frequency bands (Knyazeva et al., 2010).

Following a summary statistics approach, whole-brain synchronization maps were computed for each subject by averaging over all available epochs. To control for interindividual variability and to decouple regional synchronization from global synchronization level in individual subjects, each map was normalized by its global mean, i.e., the spatial average of synchronization was subtracted from each local S-estimator in each 1-second epoch. Such normalization assumes an equality of global mean values across samples, which was the case for the baseline versus 1-year sessions in both groups, but not for patients versus controls (2-way analysis of variance [ANOVA] with disease [AD patients vs. controls] and observation period [baseline and 1-year session] factors). Because our study was primarily focused on the evolution of EEG synchronization, we used the normalization to unmask regions with the greatest rate of AD-related progression. However, to avoid misinterpretations due to significantly lower mean synchronization levels in patients ($p < 0.01$), we also analyzed nonnormalized data. The so obtained absolute and relative synchronization maps entered a population analysis.

We acknowledge the fact that localization of distributed sources based on the LAURA algorithm has limited spatial resolution, because field spread is not completely abolished in source space (Schoffelen and Gross, 2009). This is a consequence of the high indeterminacy of the inverse problem and of the approximations in modeling head geometry and spatial conductivity in the forward model. As a result, source signals are not perfectly reconstructed and spatially localized and may result in spurious values of the S-estimator. Given our high-density EEG setup (> 100 channels), the localization accuracy with LAURA is in the order of the grid size, i.e., about 1 cm (Michel et al., 2004). Furthermore, the whole-brain maps of source power minimize the possibility that our synchronization maps depend significantly on signal-to-noise ratio changes (see Supplementary data). Finally, as described in the following paragraph, we applied a conservative statistical approach in order to interpret only the most pronounced effects.

2.6. Group statistics

Two-way between-within ANOVAs included disease (AD patients vs. controls) as a first factor and observation period (2 levels: t_0 and t_1 at baseline and 1-year session, respectively) as a second. Two-way between-within ANOVAs were also performed on the AD patients separately. With this design we analyzed the effects of AD subtype (fast-progressing patients vs. slow-progressing patients), observation period (2 levels: t_0 and t_1), and their interaction. Interactions were sought with planned comparisons that contrasted t_0 and t_1 data separately in patients and controls (the first ANOVA) and in the 2 subgroups of patients (the second ANOVA).

To reduce the computational burden of permutation-based nonparametric testing, we applied a parametric ANOVA based on the Gaussian distribution. According to the central limit theorem, because our summary statistics at the between-subject level are linear mixtures of within-

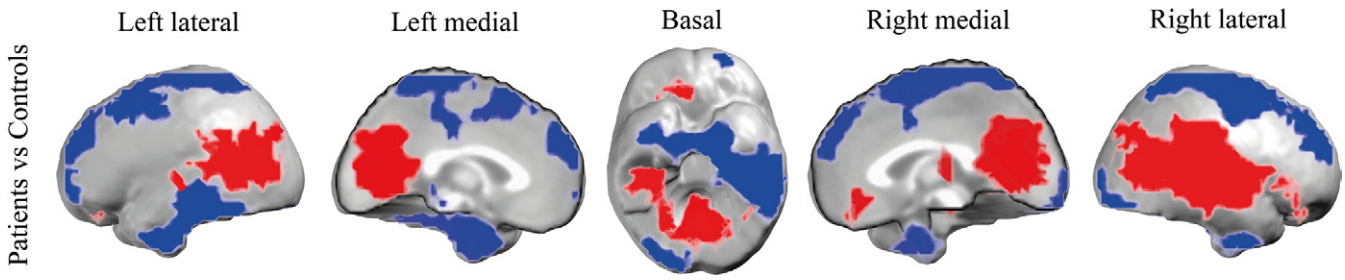

Fig. 1. Main effect of Alzheimer's disease on regional multivariate synchronization. The whole-brain 3-D rendering for the S-estimator shows clusters of sources hypersynchronized (in red) and hyposynchronized (in blue) in patients compared with control subjects independently of the electroencephalogram (EEG) recording session. The effects were considered significant at local false discovery rate (lfdr) ≤ 0.1 for clusters ≥ 5 sources. In the gray areas there were no significant effects. For details see the Results section. All the maps were made with Cartool software (https://sites.google.com/site/fbmlab/cartool), which displays the solution points as a series of transparent iso-surfaces. To render the significant effect at a deep source, a shift between its real position and surface projection was used. Specifically, deep sources were displayed on top of superficial sources. For medial views, we applied a light shift (up to 12% of the maximum depth, i.e., the depth of 1 hemisphere of the Montreal Neurological Institute's [MNI] average brain), while for other views we applied a medium shift (25% of the maximum depth).

subject level data, the random errors in such ANOVAs are well approximated by a Gaussian distribution.

The univariate p-values were controlled for whole-brain multiple testing through the local false discovery rate (lfdr) approach (Efron, 2004). The lfdr controls the expected proportion of significant findings that are indeed false positives (type I errors). It is an empirical Bayesian method and is defined from a 2-component mixture model of the observed p-value distribution, namely:

$$f(P) = \eta_0 f_0(P) + (1 - \eta_0) f_A(P)$$

where the null density f_0 is the uniform distribution $U(0,1)$, which corresponds to the p-values of no interest, f_A is an alternative density for the p-values of interest, η_0 is a true null proportion, which is estimated from the computed p-value distribution together with the alternative density f_A. The lfdr is defined as:

$$lfdr(P) = \frac{\eta_0 f_0(P)}{f_A(P)}$$

This formula provides the probability that a null hypothesis is true given the corresponding p-value. Contrary to traditional false discovery methods (Strimmer, 2008), this approach takes into account dependencies between multiple null hypotheses. In our case, it also accommodates spatial dependences across a whole-brain synchronization map.

We computed the lfdr from the distribution of p-values obtained for the 4024 null hypotheses under test via an estimator implemented in the software package fdrtool (http://cran.r-project.org/web/packages/fdrtool/index.html). Solution points with a conservative lfdr ≤ 0.1 (c.f., with a conventional lfdr ≤ 0.2) were considered significant.

The results of ANOVAs are described as the percentage of solution points with significant changes of S-estimator for broadband source EEG relative to the total number of solution points spanning relevant anatomical structures, based on the source grid (see Section 2.3.).

3. Results

An ANOVA on nonnormalized data with disease and observation period as factors (see Methods section for details) showed a significant effect of disease but no effect of time, nor any interaction. The main effect of disease showed up as a synchronization reduction across all solution points (lfdr ≤ 0.1). Therefore, nonnormalized data failed to localize AD-affected brain regions or to follow AD progression.

The main effect of disease on normalized S-maps manifested itself in both hemispheres (blue clusters in Fig. 1, Supplementary Table 1) as both hyper- and hyposynchronized clusters. Hyposynchronized clusters in patients were located in the temporal and prefrontal cortices. The most affected territories included the superior, middle, and medial frontal gyri bilaterally (20%–40%, the percentage is relative to the total number of sources spanning respective anatomical structure based on the source grid) and the left inferior and middle temporal gyri (13%–47%). In the medial temporal lobe, the uncus (bilaterally, 20%–54% of sources), and the left parahippocampal gyrus (18%) together with the left fusiform gyrus (27%) were affected.

Hypersynchronization was found in posterior clusters located on the medial, basal, and lateral surfaces of both hemispheres (red clusters in Fig. 1) with the largest hypersynchronized network on the right hemispheric convexity. This cluster spread from the right inferior and middle occipital gyri posteriorly to the precentral and middle frontal gyri anteriorly, thus covering a significant part of the lateral temporal territories including the superior (57% of sources), middle (33%), and transverse (86%) temporal gyri and the right insula (70%) (Supplementary Table 1). In the left hemisphere, the hypersynchronized cluster was limited to the parietal and temporal cortices including parts of the superior and middle temporal gyri (31% and 20% of sources, respectively), and of the supramarginal gyrus (21%).

The medial hemispheric surfaces were affected symmetrically. Hypersynchronized networks covered the posterior cingulate gyrus (51%–69% of sources), precuneus (37%–42%), and cuneus (53%–57%). On the basal hemispheric surface they were found in the lingual (31%–36% of sources), right fusiform (11%), and right parahippocampal (30%) gyri. Neither the main effect of time nor the interaction was significant.

Because heterogeneity of AD progression was a probable cause for the failure to show AD-specific changes in EEG synchronization with time, we repeated this analysis after dividing our patients into 2 sets characterized by fast- (RAD group, 8 patients) or slow progression (SAD group, 7 patients) of AD symptoms in the period of observation (Table 1b). As seen in the table, at baseline the 2 AD subgroups did not differ significantly in age, MMSE score, or the duration of AD symptoms. Over the period of clinical observation (2 years on average) the MMSE score dropped in the RAD group ($p < 0.001$), but did not change significantly in the SAD group. The between-subgroup difference in MMSE was significant both at first-year (t_1) ($p < 0.005$; not given in the table) and second-year examination ($p < 0.001$). We used this categorization for a 2-way between-within ANOVA to explore the main effects and interaction between AD subtypes (RAD vs. SAD) and period between EEGs (t_1 vs. t_0). We found no significant main effects or interaction, when analyzing nonnormalized data.

For normalized data, despite the absence of main effects, we found a significant interaction between AD subtype and time, revealing cortical territories in which synchronization changed differentially in RAD compared with SAD patients (Fig. 2, top row; Supplementary Table 2). The differences were much more widespread in the left hemisphere occupying frontal and temporal cortices, including the inferior frontal gyrus (31% of sources) together with adjacent territories in the precentral (20%), middle frontal (15%), superior temporal (13%), and middle temporal (4%) gyri. The left medial temporal lobe was among the most affected regions. Clusters of deviant synchronization were located prominently in the uncus (79% of sources) and the parahippocampal gyrus (30%). The posterior cingulate was affected bilaterally (10%–41%). Another cluster was located in the distal part of the left precentral gyrus.

To interpret the interaction, we examined simple main effects with planned comparisons between the 2 sessions (t_1 vs. t_0) separately in RAD and SAD patients. The results of these comparisons show frontotemporal hypo-synchronization in the RAD subgroup over a year (Fig. 2, bottom row). These effects were seen predominantly in the left hemisphere. Seventy-one percent of sources were affected in the uncus, 25% in the parahippocampal gyrus, 28% in the inferior frontal gyrus and 14%, in the middle frontal gyrus. There were also small clusters of increased synchronization located in the precentral and posterior cingulate gyri bilaterally and in the left subcallosal gyrus and left precuneus. SAD patients showed no significant changes in source EEG synchronization over a year.

To better understand regional dynamics exposed by hypersynchronized clusters in normalized maps, we visualized a synchronization landscape in absolute values of S-estimator (Fig. 3A). As this figure demonstrates, the landscape is characterized by peak values of S-estimator in the parietal/cingulate regions in both groups and by dip values in the medial temporal regions. We also performed a 3-way ANOVA with disease (AD vs. controls), observation period (t_0 vs. t_1) and cluster type (hyper- vs. hyposynchronized) factors on absolute values of the S-estimator averaged over the clusters outlined in Fig. 3A. They showed up both in the

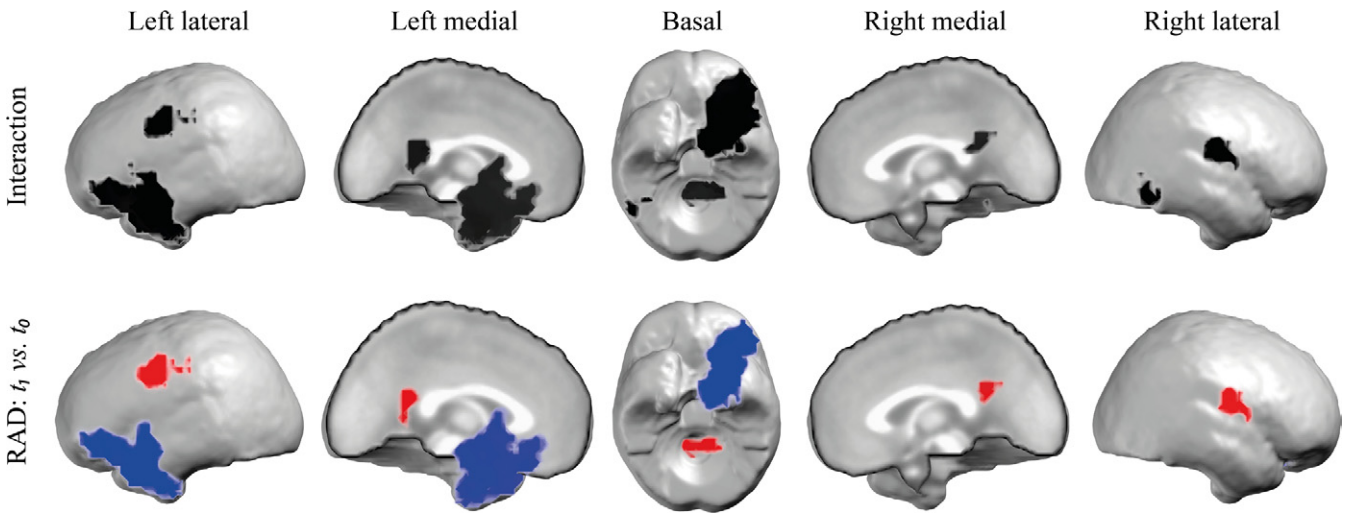

Fig. 2. Interaction between progression of Alzheimer's disease and time. The top row shows the 3-D rendering of interaction effects on the S-estimator. Black areas correspond to the significant interaction effects at local false discovery rate (lfdr) ≤ 0.1. The bottom row shows the planned simple contrast t_1 versus t_0 in Alzheimer's disease (AD) patients with rapidly progressing disease. Blue color corresponds to $t_1 < t_0$, while red color corresponds to $t_1 > t_0$. For details see the Results section.

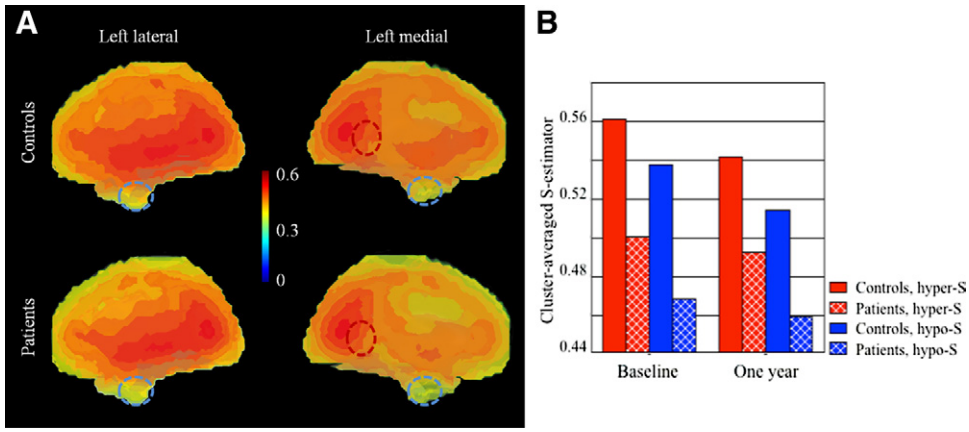

Fig. 3. (A) Topography of absolute synchronization. The whole-brain landscape of absolute S-estimator values is shown for recordings at the baseline session. A cool-warm color scale represents low-high values of synchronization. The 3-D maps of the left hemisphere were rendered with Cartool software (https://sites.google.com/site/fbmlab/cartool) as described in Fig. 1. The blue and red ellipses highlight regions of relative hypo- and hypersynchronization (12 and 21 sources, respectively) that are common to the main effect of Alzheimer's disease (AD) (Fig. 1) and the interaction (Fig. 2). (B) Interaction effects on absolute values of S-estimator averaged for clusters outlined in (A). A significant cluster by time interaction: hypersynchronized clusters (red bars) change more slowly with time ($p = 0.023$) and a cluster by disease interaction: the difference in synchronization level between the cluster types is greater in patients ($p = 0.026$).

main effect of AD (Fig. 1) and as an interaction (Fig. 2). For nonnormalized data, we found a significant cluster by observation period interaction (hypersynchronized clusters changed more slowly with time at $p = 0.023$) and a cluster by disease interaction (the difference in synchronization levels between cluster types was greater in patients at $p = 0.026$ [Fig. 3B]).

We additionally performed a whole-brain analysis of source EEG power (see Supplementary information and Supplementary Fig. 1) with the 2 ANOVAs applied to the synchronization maps. In contrast to regionally specific changes of the S-estimator, we found either a highly dispersed decrease in absolute (i.e., nonnormalized) source EEG power in AD patients versus controls or no significant effects (RAD vs. SAD patients). This makes a significant effect of signal-to-noise ratio changes on the S-estimator very unlikely, so supporting the interpretation of our findings in terms of true regional FC.

4. Discussion

The year following clinical diagnosis is of particular importance as it is a period when a treatment is often prescribed and its effects must be tracked and estimated accurately. Here we report changes in local intraregional FC induced by mild AD and their evolution over a year. Our results suggest that such an EEG measure has potential as a biomarker of disease progression.

Some of our AD patients belonged to a larger group analyzed in a cross-sectional study (Knyazeva et al., 2010). At the point of clinical diagnosis, the whole group was characterized by a specific landscape of synchronization changes derived from high-density EEG in sensor space. This included hyposynchronized clusters in the left fronto-temporal region and hypersynchronized ones in temporo-parieto-occipital regions bilaterally. This pattern of changes was reproducible across different measures of EEG synchronization and across frequency bands. However, surface topography provides limited information about source brain structures causing the changes in EEG synchronization and therefore, limits compatibility of EEG data with results from other neuroimaging domains.

To ensure the integration of EEG-based local FC findings with other neuroimaging modalities, we applied a source EEG reconstruction with the LAURA algorithm. This allowed us to reproduce our earlier main findings, including bidirectional changes of intraregional FC in source space. In general, the distribution of regions with aberrant synchronization corresponds to brain regions known to be implicated in AD, including the medial temporal lobe and the posterior cingulate—key regions supporting memory function—as well as the lateral parietal and medial frontal areas (Braak and Braak, 1991; Buckner et al., 2005; Thompson et al., 2003, 2007).

However, our finding that in mild AD the frontal and temporal networks show reduced synchronization, while posterior networks are hypersynchronized requires special consideration. To the best of our knowledge, we were the first to show such a landscape of changes in local intraregional synchronization; a finding that is discrepant with other EEG reports and discussed in detail by Knyazeva et al. (2010) previously and so not reprised here. We suggested that local hypersynchronization is a transient event and proposed a 2-phase scenario for the evolution of FC with AD progression. Our idea was that an increase in temporal coordination of EEG activity is characteristic of early and possibly preclinical AD. With progression, ongoing degra-

dation of anatomical connectivity ultimately results in hyposynchronization. Our new results support such a scenario.

4.1. AD networks with decreased synchronization: links to other neuroimaging data

The networks with decreased intraregional synchronization are in the lateral and medial temporal regions including parahippocampal and fusiform gyri of the left hemisphere and the uncus, which is affected early in AD, and is bilaterally desynchronized. Such networks were also localized along the interhemispheric fissure, on the convexity and medial surfaces of both hemispheres from superior and medial frontal gyri to the postcentral gyrus and paracentral lobule, respectively.

The finding of hyposynchronized networks is an expected result within mainstream thinking about FC in AD. The novel aspect we add is that based on source EEG we localize these clusters to brain regions involved early in AD, thus confirming their disease-specific topography. The accumulation of neurofibrillary tangles starts in the medial temporal regions (Braak and Braak, 1991). In vivo neuroimaging and postmortem anatomical studies consistently show that brain atrophy first develops in the medial temporal lobe and then spreads across the association neocortices. These neuropathological changes manifest with gray matter (Li et al., 2011; Schuff et al., 2009; Thompson et al., 2003, 2007) and white matter (Fornari et al., 2012) loss. The latter can thus be linked to impaired FC as indeed shown in Babiloni et al. (2006b) and Knyazeva et al. (2009).

The asymmetry of hyposynchronization with greater effects in the left hemisphere is mirrored by a comparable spatial pattern of demyelination of juxtacortical white matter (Fornari et al., 2012). The juxtacortical white matter consists mostly of association U-fibers that implement local corticocortical connectivity. The deterioration of synchronization over a year (see section 4.3.) occurred in the same and neighboring areas of the left hemisphere. Thompson et al. (2003) found similar asymmetric gray matter atrophy in AD patients. Moreover, the rate of loss at follow-up was greater in the left hemisphere. These structural findings are compatible with our functional ones. Although mounting data show that the left hemisphere is more affected in early AD (Fornari et al., 2012; Thompson et al., 1998; Loewenstein et al., 1989; Thompson et al., 2003; Zhang et al., 2010), there is no explanation for this finding so far. Other neurodegenerative diseases, e.g., Parkinson's disease also show asymmetrical changes at onset.

4.2. What is so special about relatively hypersynchronized EEG networks?

The relatively hypersynchronized clusters in the normalized maps emphasize some regional features hidden in the nonnormalized data. Firstly, these networks have the highest absolute FC as demonstrated by the landscapes with the peak parietal/cingulate and the dip mediotemporal S-estimator values in our control and patient groups. An fMRI-based analysis of FC similarly showed that the posterior cingulate and lateral parietal cortices are among regions with the highest connectivity (Buckner et al., 2009). Secondly, they are characterized by a less rapid decline of FC than the medial temporal networks. Therefore, while global synchronization was lower in our AD group than in controls, there existed a differential spatial pattern with parietal and cingulate regions showing somewhat greater synchronization and a slower decline than the frontotemporal ones.

On the other hand, our results confirm that clinical manifestations of AD are associated with already impaired FC and leave open an issue of AD-related absolute increases. Because the latter were observed in a cross-sectional study of newly diagnosed AD patients (Knyazeva et al., 2010), this effect may characterize the earlier stages of disease. Indeed, recent fMRI-based studies of FC report bidirectional changes in mild AD (Damoiseaux et al., 2012; He et al., 2007; Wang et al., 2007; Zhang et al., 2010). However, given that normalization procedures were used at least in some of these studies (Damoiseaux et al., 2012; Zhang et al., 2010), the phenomenon requires further experimental examination in preclinical and early AD.

The posterior neocortical relatively hypersynchronized networks overlap with regions of decreased oxygen and glucose metabolism measured with 15O-positron-emission tomography and fluorodeoxyglucose (FDG)-positron-emission tomography. The latter include the lateral and medial parietal and posterior cingulate cortices, extending into lateral occipital and medial temporal regions (Buckner et al., 2005; Edison et al., 2007; Ewers et al., 2011; Frackowiak et al., 1981). Hypometabolism in parietal/posterior cingulate regions is a very early event observed at a preclinical stage, when neither cognitive deficits, nor cerebral atrophy are detected (Mosconi et al., 2008). The metabolic findings indicate declining synaptic activity that correlates with cognitive deterioration (Jack et al., 2010) and with postmortem changes of AD (Hoffman et al., 2000).

Because EEG and glucose metabolism reflect aspects of synaptic activity, the methods would be expected to produce clinically relevant spatially overlapping results, which is indeed the case. Correlations between EEG localization based on a single dipole model and spatial extent of energy hypometabolism have been demonstrated in a mixed mild cognitive impairment-AD population (Dierks et al., 2000). In a recent mouse model with a prodromal AD/mild cognitive impairment phenotype, hypometabolic regions overlap with loci of EEG change (Platt et al., 2011). Finally, a likely association between hypometabolism and intraregional EEG synchronization is supported by accumulating evidence from epilepsy studies. Sites of seizure generation and propagation demonstrate interictal glucose hypometabolism (Henry and Votaw, 2004) and an increase of interictal regional synchronization of intracranial activity, magnetoencephalographic (MEG), and EEG across a wide range of

epilepsies in both animal models and humans (Bettus et al., 2008; Douw et al., 2010; Garcia Dominguez et al., 2005; Ortega et al., 2008; Schevon et al., 2007).

Collectively these results suggest that increased EEG synchronization is a manifestation of the hypoactive state of a region in early AD. The clinical significance of this possibility is that the earliest EEG signs of preclinical AD may be hypersynchronization in the posterior cortex.

4.3. Follow-up: rapidly progressing versus slowly progressing AD

Several longitudinal studies have considered EEG/MEG as a potential objective marker of AD progression. Only a proportion of them is based on serial recordings (al Soininen et al., 1991; Coben et al., 1985; Dunkin et al., 1994; Jelic et al., 2000; Rossini et al., 2006), while in others the baseline EEG/MEG has been retrospectively used as a predictor of outcome in clinical follow-up (Luckhaus et al., 2008; Prichep, 2007; van der Hiele et al., 2008; Verdoorn et al., 2011). Reports based on power spectral analysis have consistently shown EEG slowing in AD patients, associated with a relative power decrease in the fast α and β and an increase in the δ and θ frequencies. Although well established, these EEG features lack sufficient specificity, because they are also present in other frequent pathologies encountered in elderly populations, among them multi-infarct dementia, Parkinson's disease, stroke, as well as in normal aging (Stomrud et al., 2010).

EEG source analysis was expected to improve its diagnostic specificity via the localization of power changes to regions preferentially affected by AD. Indeed, increased θ source power has been found in the temporal and parietal cortices in AD-converters (Prichep, 2007). Yet, of the 2 longitudinal studies using source EEG analysis that report medication effects, only 1 found a shift of the power spectrum after a 3-month treatment with rivastigmine in frontoparietal, posterior cingulate, and medial temporal regions (Gianotti et al., 2008), while the other failed to find any changes after a year of donepezil dosing (Babiloni et al., 2006).

Mapping synchronization of source EEG (or MEG) is an alternative approach to improving the potential of high density EEG as an AD biomarker. Although previous studies have not fully exploited the spatial dimension of EEG, because region-of-interest approaches and/or bivariate measures of synchronization suboptimal for whole-brain mapping, they have reported a number of promising findings, including the AD-specific topography of longitudinal changes and their correlation with AD progression (Prichep, 2007; Rossini et al., 2006; Verdoorn et al., 2011). In contrast to the greater accuracy of narrow-band power indicators of AD, an efficient marker of changes in functional connectivity turns out to be broadband synchronization (Knyazeva et al., 2010; Prichep, 2007; Verdoorn et al., 2011). Here we have further optimized the analysis of FC in AD by whole-brain mapping of broadband multivariate source synchronization.

The temporal dynamics of normalized synchronization appear to be sensitive to AD progression rate within the limited observation period of a year. We have demonstrated a clear interaction between synchronization changes over time and the rate of AD progression in territories affected by AD pathology. In contrast to the relatively stable AD group that showed no detectable synchronization changes, the progressing group showed both increases and decreases in regional synchronization. The major change, however, is left-lateralized hyposynchronization in the medial temporal lobe and adjacent frontal cortex that includes the uncus, parahippocampal gyrus, and inferior and middle frontal gyri, further supporting the AD specific topography of EEG synchronization changes.

In contrast, the relative increase in synchronization is localized to small bilateral areas in the posterior cingulate and precentral gyri. Three of 4 areas overlap with the hypersynchronized areas implicated by the main effect of AD. The comparisons between baseline and after a year show that although hypersynchronization is still observable in rapidly progressive AD, it is much less widespread than hyposynchronization, which may indicate flattening of regional rates of decline. A similar trend was observed by Damoiseaux et al. (2012), who showed bidirectional changes of fMRI-based connectivity in AD patients at baseline, but only reductions at follow-up.

These findings imply that normalized intraregional synchronization is a sensitive measure of AD progression and of interregional heterochronicity associated with pathological processes. As our results relate to group studies, it remains to be determined whether the sensitivity of our noninvasive and readily available technique is sufficient for individual patient monitoring.

4.4. Conclusion

The significance of EEG for AD has been relatively low because of nonspecific findings such as spectral slowing (Jeong, 2004). Our approach, based on multivariate source EEG synchronization has revealed a whole-brain, AD-specific phenotype of temporal coordination in distributed cortical networks, which shows clinically relevant changes over time. This suggests a new role for EEG as part of a multimodal imaging approach to early diagnostics and for tracking AD evolution. As a cost-effective noninvasive technique, EEG can be widely used for primary preclinical AD screening, followed by other neuroimaging techniques, if indicated. However, the limitations of this study, which include gender composition of control and patient groups and small sample size for the post hoc descriptive analysis of RAD vs. SAD subgroups, require confirmation of the results obtained and further studies designed to specify in detail the association between regional EEG synchronization and other neuroimaging modalities.

Disclosure statement

The authors disclose no conflicts of interest.

All the procedures applied in this study and described in this report conform to the Declaration of Helsinki (1964) by the World Medical Association concerning human experimentation and were approved by the local Ethics Committee of Lausanne University. All the patients, caregivers, and control subjects gave written informed consent.

Acknowledgements

This work was supported by Swiss National Foundation, Grant Number 320030-127538/1. We thank Drs. S. Gonzalez and R. Grave Peralta de Menendez for the discussions and advice on the inverse EEG solution. We are also indebted to Mme. Brioschi, Mme. Bourquin, and Mme. Moset for the neuropsychological testing of patients and controls. Finally, we greatly acknowledge all the patients and controls, who kindly agreed to participate in the study.

Appendix A. Supplementary data

Supplementary data associated with this article can be found, in the online version, at http://dx.doi.org/10.1016/j.neurobiolaging.2012.07.012.

References

Practice parameter for diagnosis and evaluation of dementia (summary statement). Report of the Quality Standards Subcommittee of the American Academy of Neurology. Neurology, 1994 44, 2203–2206.

Babiloni, C., Cassetta, E., Dal Forno, G., Del Percio, C., Ferreri, F., Ferri, R., Lanuzza, B., Miniussi, C., Moretti, D.V., Nobili, F., Pascual-Marqui, R.D., Rodriguez, G., Luca Romani, G., Salinari, S., Zanetti, O., Rossini, P.M., 2006. Donepezil effects on sources of cortical rhythms in mild Alzheimer's disease: responders vs. non-responders. Neuroimage 31, 1650–1665.

Babiloni, C., Ferri, R., Binetti, G., Cassarino, A., Dal Forno, G., Ercolani, M., Ferreri, F., Frisoni, G.B., Lanuzza, B., Miniussi, C., Nobili, F., Rodriguez, G., Rundo, F., Stam, C.J., Musha, T., Vecchio, F., Rossini, P.M., 2006a. Fronto-parietal coupling of brain rhythms in mild cognitive impairment: a multicentric EEG study. Brain Res. Bull. 69, 63–73.

Babiloni, C., Frisoni, G., Steriade, M., Bresciani, L., Binetti, G., Del Percio, C., Geroldi, C., Miniussi, C., Nobili, F., Rodriguez, G., Zappasodi, F., Carfagna, T., Rossini, P.M., 2006b. Frontal white matter volume and delta EEG sources negatively correlate in awake subjects with mild cognitive impairment and Alzheimer's disease. Clin. Neurophysiol. 117, 1113–1129.

Bettus, G., Wendling, F., Guye, M., Valton, L., Régis, J., Chauvel, P., Bartolomei, F., 2008. Enhanced EEG functional connectivity in mesial temporal lobe epilepsy. Epilepsy Res. 81, 58–68.

Birks, J., 2006. Cholinesterase inhibitors for Alzheimer's disease. Cochrane Database Syst. Rev. 25:CD005593.

Braak, H., Braak, E., 1991. Neuropathological stageing of Alzheimer-related changes. Acta Neuropathol. 82, 239–259.

Brown, R., Kocarev, L., 2000. A unifying definition of synchronization for dynamical systems. Chaos 10, 344–349.

Buckner, R.L., Snyder, A.Z., Shannon, B.J., LaRossa, G., Sachs, R., Fotenos, A.F., Sheline, Y.I., Klunk, W.E., Mathis, C.A., Morris, J.C., Mintun, M.A., 2005. Molecular, structural, and functional characterization of Alzheimer's disease: evidence for a relationship between default activity, amyloid, and memory. J. Neurosci. 25, 7709–7717.

Carmeli, C., 2006. Assessing Cooperative Behavior in Dynamical Networks With Applications to Brain Data. Available at: http://library.epfl.ch/theses/?nr=3651.

Carmeli, C., Knyazeva, M.G., Innocenti, G.M., De Feo, O., 2005. Assessment of EEG synchronization based on state-space analysis. Neuroimage 25, 339–354.

Coben, L.A., Danziger, W., Storandt, M., 1985. A longitudinal EEG study of mild senile dementia of Alzheimer type: changes at 1 year and at 2.5 years. Electroencephalogr. Clin. Neurophysiol. 61, 101–112.

Damoiseaux, J.S., Prater, K.E., Miller, B.L., Greicius, M.D., 2012. Functional connectivity tracks clinical deterioration in Alzheimer's disease. Neurobiol. Aging 33, 828.e19–30.

Dierks, T., Jelic, V., Pascual-Marqui, R.D., Wahlund, L., Julin, P., Linden, D.E., Maurer, K., Winblad, B., Nordberg, A., 2000. Spatial pattern of cerebral glucose metabolism (PET) correlates with localization of intracerebral EEG-generators in Alzheimer's disease. Clin. Neurophysiol. 111, 1817–1824.

Douw, L., de Groot, M., van Dellen, E., Heimans, J.J., Ronner, H.E., Stam, C.J., Reijneveld, J.C., 2010. "Functional connectivity" is a sensitive predictor of epilepsy diagnosis after the first seizure. PLoS One 5, e.10839.

Dunkin, J.J., Leuchter, A.F., Newton, T.F., Cook, I.A., 1994. Reduced EEG coherence in dementia: state or trait marker? Biol. Psychiatry 35, 870–879.

Edison, P., Archer, H.A., Hinz, R., Hammers, A., Pavese, N., Tai, Y.F., Hotton, G., Cutler, D., Fox, N., Kennedy, A., Rossor, M., Brooks, D.J., 2007. Amyloid, hypometabolism, and cognition in Alzheimer disease: an [11C]PIB and [18F]FDG PET study. Neurology 68, 501–508.

Efron, B., 2004. Large-scale simultaneous hypothesis testing: the choice of a null hypothesis. J. Am. Stat. Assoc. 99, 96–104.

Ewers, M., Frisoni, G.B., Teipel, S.J., Grinberg, L.T., Amaro, E.Jr., Heinsen, H., Thompson, P.M., Hampel, H., 2011. Staging Alzheimer's disease progression with multimodality neuroimaging. Prog. Neurobiol. 95, 535–546.

Folstein, M.F., Folstein, S.E., McHugh, P.R., 1975. "Mini-mental state". A practical method for grading the cognitive state of patients for the clinician. J. Psychiatr. Res. 12, 189–198.

Fornari, E., Maeder, P., Meuli, R., Ghika, J., Knyazeva, M.G., 2012. Demyelination of superficial white matter in early Alzheimer's disease: a magnetization transfer imaging study. Neurobiol. Aging 33, 428e7.–19.

Frackowiak, R.S., Pozzilli, C., Legg, N.J., Du Boulay, G.H., Marshall, J., Lenzi, G.L., Jones, T., 1981. Regional cerebral oxygen supply and utilization in dementia. A clinical and physiological study with oxygen-15 and positron tomography. Brain 104, 753–778.

Friston, K.J., Frith, C.D., Frackowiak, R.S.J., 1993. Time dependent changes in effective connectivity measured with PET. Hum. Brain Mapp. 1, 69–80.

Garcia Dominguez, L., Wennberg, R.A., Gaetz, W., Cheyne, D., Snead, O.C., III, Perez Velazquez, J.L., 2005. Enhanced synchrony in epileptiform activity? Local versus distant phase synchronization in generalized seizures. J. Neurosci. 25, 8077–8084.

Gianotti, L.R., Künig, G., Faber, P.L., Lehmann, D., Pascual-Marqui, R.D., Kochi, K., Schreiter-Gasser, U., 2008. Rivastigmine effects on EEG spectra and three-dimensional LORETA functional imaging in Alzheimer's disease. Psychopharmacology (Berl.) 198, 323–332.

Grave de Peralta Menendez, R., Gonzalez Andino, S., Lantz, G., Michel, C.M., Landis, T., 2001. Noninvasive localization of electromagnetic epileptic activity. I. Method descriptions and simulations. Brain Topogr. 14, 131–137.

Grave de Peralta Menendez, R., Morier, P., Picard, F., Landis, T., Gonzalez Andino, S.L., 2006. Simple techniques for EEG source imaging. Int. J. Bioelectromagnet. 8, 1–8.

Guggisberg, A.G., Dalal, S.S., Zumer, J.M., Wong, D.D., Dubovik, S., Michel, C.M., Schnider, A., 2011. Localization of cortico-peripheral coherence with electroencephalography. Neuroimage 57, 1348–1357.

He, Y., Wang, L., Zang, Y., Tian, L., Zhang, X., Li, K., Jiang, T., 2007. Regional coherence changes in the early stages of Alzheimer's disease: a combined structural and resting-state functional MRI study. Neuroimage 35, 488–500.

Henry, T.R., Votaw, J.R., 2004. The role of positron emission tomography with [18F]fluorodeoxyglucose in the evaluation of the epilepsies. Neuroimaging Clin. N. Am. 14, 517–535.

Hoffman, J.M., Welsh-Bohmer, K.A., Hanson, M., Crain, B., Hulette, C., Earl, N., Coleman, R.E., 2000. FDG PET imaging in patients with pathologically verified dementia. J. Nucl. Med. 41, 1920–1928.

Jack, C.R., Jr., Knopman, D.S., Jagust, W.J., Shaw, L.M., Aisen, P.S., Weiner, M.W., Petersen, R.C., Trojanowski, J.Q., 2010. Hypothetical model of dynamic biomarkers of the Alzheimer's pathological cascade. Lancet Neurol. 9, 119–128.

Jelic, V., Johansson, S.E., Almkvist, O., Shigeta, M., Julin, P., Nordberg, A., Winblad, B., Wahlund, L.O., 2000. Quantitative electroencephalography in mild cognitive impairment: longitudinal changes and possible prediction of Alzheimer's disease. Neurobiol. Aging 21, 533–540.

Jeong, J., 2004. EEG dynamics in patients with Alzheimer's disease. Clin. Neurophysiol. 115, 1490–1505.

Katz, S., 1983. Assessing self-maintenance: activities of daily living, mobility, and instrumental activities of daily living. J. Am. Geriatr. Soc. 31, 721–727.

Knyazeva, M.G., Fornari, E., Jalili, M., Meuli, R., Maeder, P., 2009. Abnormal EEG synchronization correlates with demyelination in Alzheimer's disease. NeuroImage 47(Suppl 1), S112.

Knyazeva, M.G., Jalili, M., Brioschi, A., Bourquin, I., Fornari, E., Hasler, M., Meuli, R., Maeder, P., Ghika, J., 2010. Topography of EEG multivariate phase synchronization in early Alzheimer's disease. Neurobiol. Aging 31, 1132–1144.

Koenig, T., Prichep, L., Dierks, T., Hubl, D., Wahlund, L.O., John, E.R., Jelic, V., 2005. Decreased EEG synchronization in Alzheimer's disease and mild cognitive impairment. Neurobiol. Aging 26, 165–171.

Kramer, M.A., Chang, F.L., Cohen, M.E., Hudson, D., Szeri, A.J., 2007. Synchronization measures of the scalp electroencephalogram can discriminate healthy from Alzheimer's subjects. Int. J. Neural Syst. 17, 61–69.

Lawton, M.P., Brody, E.M., 1969. Assessment of older people: self-maintaining and instrumental activities of daily living. Gerontologist 9, 179–186.

Li, X., Coyle, D., Maguire, L., Watson, D.R., McGinnity, T.M., 2011. Gray matter concentration and effective connectivity changes in Alzheimer's disease: a longitudinal structural MRI study. Neuroradiology 53, 733–748.

Lizio, R., Vecchio, F., Frisoni, G.B., Ferri, R., Rodriguez, G., Babiloni, C., 2011. Electroencephalographic rhythms in Alzheimer's disease. Int. J. Alzheimers Dis. 2011, 927573.

Loewenstein, D.A., Barker, W.W., Chang, J.Y., Apicella, A., Yoshii, F., Kothari, P., Levin, B., Duara, R., 1989. Predominant left hemisphere metabolic dysfunction in dementia. Arch. Neurol. 46, 146–152.

Luckhaus, C., Grass-Kapanke, B., Blaeser, I., Ihl, R., Supprian, T., Winterer, G., Zielasek, J., Brinkmeyer, J., 2008. Quantitative EEG in progressing vs stable mild cognitive impairment (MCI): results of a 1-year follow-up study. Int. J. Geriatr. Psychiatry 23, 1148–1155.

Mazziotta, J.C., Toga, A.W., Evans, A., Fox, P., Lancaster, J., 1995. A probabilistic atlas of the human brain: theory and rationale for its development. The International Consortium for Brain Mapping (ICBM). NeuroImage 2, 89–101.

McKhann, G., Drachman, D., Folstein, M., Katzman, R., Price, D., Stadlan, E.M., 1984. Clinical diagnosis of Alzheimer's disease: report of the NINCDS-ADRDA Work Group under the auspices of Department of Health and Human Services Task Force on Alzheimer's Disease. Neurology 34, 939–944.

Michel, C.M., Murray, M.M., Lantz, G., Gonzalez, S., Spinelli, L., Grave de Peralta, R., 2004. EEG source imaging. Clin. Neurophysiol. 115, 2195–2222.

Morris, J.C., 1993. The clinical dementia rating (CDR): current version and scoring rules. Neurology 43, 2412–2414.

Mosconi, L., Pupi, A., De Leon, M.J., 2008. Brain glucose hypometabolism and oxidative stress in preclinical Alzheimer's disease. Ann. N. Y. Acad. Sci. 1147, 180–195.

Ortega, G.J., Menendez de la Prida, L., Sola, R.G., Pastor, J., 2008. Synchronization clusters of interictal activity in the lateral temporal cortex of epileptic patients: intraoperative electrocorticographic analysis. Epilepsia 49, 269–280.

Palop, J.J., Mucke, L., 2010. Amyloid-beta-induced neuronal dysfunction in Alzheimer's disease: from synapses toward neural networks. Nat. Neurosci. 13, 812–818.

Pascual-Marqui, R.D., 2009. Theory of the EEG inverse problem, in: Tong, S., Thakor, N. (Eds.), Quantitative EEG Analysis: Methods and Clinical Applications. Artech House, Boston, pp. 121–140.

Platt, B., Drever, B., Koss, D., Stoppelkamp, S., Jyoti, A., Plano, A., Utan, A., Merrick, G., Ryan, D., Melis, V., Wan, H., Mingarelli, M., Porcu, E., Scrocchi, L., Welch, A., Riedel, G., 2011. Abnormal cognition, sleep, EEG and brain metabolism in a novel knock-in Alzheimer mouse, PLB1. PLoS One 6(11):e27068.

Prichep, L.S., 2007. Quantitative EEG and electromagnetic brain imaging in aging and in the evolution of dementia. Ann. N. Y. Acad. Sci. 1097, 156–167.

Puel, M., Hugonot-Diener, L., 1996. Presenting by the GRECO group of the French adaptation of a cognitive assessment scale used in Alzheimer type dementia. Presse Med. 22, 1028–1132.

Rossini, P.M., Del Percio, C., Pasqualetti, P., Cassetta, E., Binetti, G., Dal Forno, G., Ferreri, F., Frisoni, G., Chiovenda, P., Miniussi, C., Parisi, L., Tombini, M., Vecchio, F., Babiloni, C., 2006. Conversion from mild cognitive impairment to Alzheimer's disease is predicted by sources and coherence of brain electroencephalography rhythms. Neuroscience 143, 793–803.

Rytsar, R., Fornari, E., Frackowiak, R.S., Ghika, J.A., Knyazeva, M.G., 2011. Inhibition in early Alzheimer's disease: an fMRI-based study of effective connectivity. Neuroimage 57, 1131–1139.

Scaln, S.G., Reisberg, B., 1992. Functional Assessment Staging (FAST) in Alzhiemer's disease: reliability, validity and ordinality. Int. Psychogeriatr. 4, 55–69.

Schevon, C.A., Cappell, J., Emerson, R., Isler, J., Grieve, P., Goodman, R., McKhann, G., Jr., Weiner, H., Doyle, W., Kuzniecky, R., Devinsky, O., Gilliam, F., 2007. Cortical abnormalities in epilepsy revealed by local EEG synchrony. Neuroimage 35, 140–148.

Schoffelen, J.M., Gross, J., 2009. Source connectivity analysis with MEG and EEG. Hum. Brain Mapp. 30, 1857–1865.

Schuff, N., Woerner, N., Boreta, L., Kornfield, T., Shaw, L.M., Trojanowski, J.Q., Thompson, P.M., Jack, C.R., Jr., Weiner, M.W., Alzheimer's Disease Neuroimaging Initiative, 2009. MRI of hippocampal volume loss in early Alzheimer's disease in relation to ApoE genotype and biomarkers. Brain 132, 1067–1077.

Schuz, A., Braitenberg, V., 2002. The human cortical white matter: Quantitative aspects of cortico-cortical long-range connectivity, in: Schultz, R., Miller, R. (Eds.), Cortical Areas: Unity and Diversity (Conceptual Advances in Brain Research). Taylor & Francis, London, pp. 377–386.

Singer, W., 1999. Neuronal synchrony: a versatile code for the definition of relations? Neuron 24, 49–65, 111–125.

Soininen, H., Partanen, J., Laulumaa, V., Pääkkönen, A., Helkala, E.L., Riekkinen, P.J., 1991. Serial EEG in Alzheimer's disease: 3 year follow-up and clinical outcome. Electroencephalogr. Clin. Neurophysiol. 79, 342–348.

Sperling, R.A., Dickerson, B.C., Pihlajamaki, M., Vannini, P., LaViolette, P.S., Vitolo, O.V., Hedden, T., Becker, J.A., Rentz, D.M., Selkoe, D.J., Johnson, K.A., 2010. Functional alterations in memory

networks in early Alzheimer's disease. Neuromolecular Med. 12, 27–43.

Stam, C.J., Montez, T., Jones, B.F., Rombouts, S.A., van der Made, Y., Pijnenburg, Y.A., Scheltens, P., 2005. Disturbed fluctuations of resting state EEG synchronization in Alzheimer's disease. Clin. Neurophysiol. 116, 708–715.

Stomrud, E., Hansson, O., Minthon, L., Blennow, K., Rosén, I., Londos, E., 2010. Slowing of EEG correlates with CSF biomarkers and reduced cognitive speed in elderly with normal cognition over 4 years. Neurobiol. Aging 31, 215–223.

Strimmer, K., 2008. A unified approach to false discovery rate estimation. BMC Bioinformatics 9, 303.

Thompson, P.M., Moussai, J., Zohoori, S., Goldkorn, A., Khan, A.A., Mega, M.S., Small, G.W., Cummings, J.L., Toga, A.W., 1998. Cortical variability and asymmetry in normal aging and Alzheimer's disease. Cereb. Cortex 8, 492–509.

Thompson, P.M., Hayashi, K.M., de Zubicaray, G., Janke, A.L., Rose, S.E., Semple, J., Herman, D., Hong, M.S., Dittmer, S.S., Doddrell, D.M., Toga, A.W., 2003. Dynamics of gray matter loss in Alzheimer's disease. J. Neurosci. 23, 994–1005.

Thompson, P.M., Hayashi, K.M., Dutton, R.A., Chiang, M.C., Leow, A.D., Sowell, E.R., De Zubicaray, G., Becker, J.T., Lopez, O.L., Aizenstein, H.J., Toga, A.W., 2007. Tracking Alzheimer's disease. Ann. N. Y. Acad. Sci. 1097, 183–214.

van der Hiele, K., Bollen, E.L., Vein, A.A., Reijntjes, R.H., Westendorp, R.G., van Buchem, M.A., Middelkoop, H.A., van Dijk, J.G., 2008. EEG markers of future cognitive performance in the elderly. J. Clin. Neurophysiol. 25, 83–89.

Verdoorn, T.A., McCarten, J.R., Arciniegas, D.B., Golden, R., Moldauer, L., Georgopoulos, A., Lewis, S., Cassano, M., Hemmy, L., Orr, W., Rojas, D.C., 2011. Evaluation and tracking of Alzheimer's disease severity using resting-state magnetoencephalography. J. Alzheimers Dis. 26(Suppl 3), 239–255.

Wang, K., Liang, M., Wang, L., Tian, L., Zhang, X., Li, K., Jiang, T., 2007. Altered functional connectivity in early Alzheimer's disease: a resting-state fMRI study. Hum. Brain Mapp. 28, 967–978.

Zhang, H.Y., Wang, S.J., Liu, B., Ma, Z.L., Yang, M., Zhang, Z.J., Teng, G.J., 2010. Resting brain connectivity: changes during the progress of Alzheimer disease. Radiology 256, 598–606.